Electrochemistry Communications 112 (2020) 106675

Contents lists available at ScienceDirect

Electrochemistry Communications

journal homepage: www.elsevier.com/locate/elecom

A volume of fluid (VOF) method to model shape change during electrodeposition

E. Karimi-Sibaki[a], A. Kharicha[a,*], A. Vakhrushev[a], M. Wu[b], A. Ludwig[b], J. Bohacek[b]

[a] Christian-Doppler Laboratory for Metallurgical Applications of Magnetohydrodynamics, Montanuniversitaet of Leoben, Franz-Josef-Str. 18, A-8700 Leoben, Austria
[b] Chair of Simulation and Modeling of Metallurgical Processes, Montanuniversitaet of Leoben, Franz-Josef-Str. 18, A-8700 Leoben, Austria

ARTICLE INFO

Keywords:
Shape change
Numerical simulation
VOF interface area
Secondary current distribution
Electroforming

ABSTRACT

A novel volume of fluid (VOF) based approach is proposed to simulate the transient shape change of deposit front during electrodeposition considering secondary current distribution. Transport phenomena such as electrolyte potential, electric current density, and fluid flow of electrolyte are computed. The presented algorithm comprises computation of the exact VOF interface area as well as proposed modeling equations to accurately handle transport phenomena within the deposit. Based on the modeling results, it is essential to minimize the overshoot of electric current near the singularity between the cathode and insulator in the beginning stages of electrodeposition to achieve a relatively uniform thickness of the deposit layer in electroforming process. The results are validated against existing mathematical solutions.

1. Introduction

Electrodeposition is a popular technique to produce metals, alloys and composite materials. The electrodeposition cell contains an electrolyte and two electrodes, namely the anode and cathode. The electrolyte as an ionic conductor is in the liquid state where the metal of interest (e.g. copper, silver, gold, zinc, nickel, chromium, etc.) participates in faradaic reduction reaction. The metal ion converts to metal atom at the cathode surface where a continuously growing metal deposit layer forms [1,2].

Electrodeposition is a multiphase and multiphysics problem involving the interplay of several transport phenomena such as heat transfer, mass transfer, electric current density, ion concentrations, and the interaction between flow and magnetic field known as magnetohydrodynamics (MHD) [3–5]. Most often, the thickness and shape (profile) of the deposit metal are used as an indicator to evaluate the performance of the process. Thus, it is of great importance to develop transient models aiming at tracking the deposit front and computing transport phenomena.

The distribution of electric current density is a decisive parameter in the electrodeposition process [6]. Three classes are recognized, namely primary, secondary, and tertiary current distribution [7–9]. Here, we utilize the secondary current distribution in which the composition variation in the electrolyte is ignored, whereas the electrode kinetics at the deposit front is accounted for through the Butler–Volmer formula [9].

Over the past decades, the finite element method (FEM) [10–12] or finite difference method (FDM) [13–16] were extensively used to discretize governing partial differential equations (PDE) related to electrodeposition phenomenon. Various methods such as phase field modeling [17,18], Monte Carlo technique [19], boundary element method (BEM) [12], level set method [12–14], and dynamic mesh [20,21] technique were proposed. Phase field and Monte Carlo require thermodynamics data of free energy or entropy, and they can only work well on a small scale (up to several micrometers) with the current computational resources. BEM is not applicable for all ranges of nonlinear problems (e.g. in presence of flow) [22]. Dynamic mesh is recommended for problems involving unidirectional deformation of boundaries. Level set requires a transition zone (diffuse interface) around the interface to specify a smooth function. The transition zone covers several computational cells spanning the exact location of the interface. The shape of function must remain the same as the interface so that re-initialization of the function is essential at each time step.

Here, we propose a novel transient approach using volume of fluid (VOF) [23]. Unlike level set, the proposed VOF-based method does not require a diffuse interface, as the thickness of the deposit–electrolyte interface remains one computational cell. It is capable of simulating any complex shape change of the deposit front regardless of the scale of process. VOF as a well-known, powerful numerical technique in computational fluid dynamics (CFD) tracks the volume fraction of each

---

[*] Corresponding author.
E-mail address: abdellah.kharicha@unileoben.ac.at (A. Kharicha).

https://doi.org/10.1016/j.elecom.2020.106675
Received 9 December 2019; Received in revised form 17 January 2020; Accepted 27 January 2020

Nomenclature

a	cell size, m
a_{VOF}	interface area, m
F	Faraday constant, A s mol^{-1}
g	gravity constant, m s^{-2}
$\vec{j}$	electric current density, A m^{-2}
j_0	exchange current density, A m^{-2}
j_{BV}	current density of Butler–Volmer, A m^{-2}
j_{ave}	average current density, A m^{-2}
K	permeability
L	characteristic length, m
$\dot{m}$	mass source, kg m^{-3} s^{-1}
M	molecular weight, g mol^{-1}
$\vec{n}\,(n_{\mathrm{x}}, n_{\mathrm{y}})$	unit normal vector
p	pressure, Pa
R	universal gas constant, J K^{-1} mol^{-1}
S_{u}	momentum sink term, N m^{-3} s^{-1}
S_{φ}	potential sink term, A m^{-3} s^{-1}
t	time, s
T	temperature, K
$\vec{u}$	velocity vector, m s^{-1}
u_0	inlet velocity, m s^{-1}
u_{df}	deposit front velocity, m s^{-1}
V	volume of computational cell, m^3
V_{d}	deposit volume in computational cell, m^3
$\vec{x}$	vector coordinates, m
x, y	coordinates, m
X, Y	dimensionless coordinates
z	number of exchanged electrons
α	charge transfer coefficient
β	volume fraction of deposit
β_{L}	limit volume fraction of deposit
δ	length scale, m
ρ	density, kg m^{-3}
ρ_{d}	deposit density, kg m^{-3}
ρ_{e}	electrolyte density, kg m^{-3}
μ	dynamic viscosity, kg s^{-1} m^{-1}
μ_{d}	deposit viscosity, kg s^{-1} m^{-1}
μ_{e}	electrolyte viscosity, kg s^{-1} m^{-1}
φ	electrolyte potential, V
φ_{int}	overpotential, V
κ	electrical conductivity, S m^{-1}
Δt	time step size, s
$()^*$	a normalized parameter

phase (i.e. deposit and electrolyte) throughout the domain. Furthermore, VOF enables us to fully resolve transport phenomena [23–26]. All governing equations are discretized using the finite volume method (FVM) that automatically conserves mass, momentum and energy [27].

The model is examined on two systems, namely unidirectional [28] and multidirectional [10] deformation, which closely resembles the process of electroforming [29] (see Fig. 1). Transient profile of deposit front as well as transport phenomena are calculated considering secondary current distribution. The proposed VOF model can be used in a cost effective way to enhance our knowledge on the transient behavior of the electrodeposition process and to provide guidelines for the optimal design of electrodeposition cell and operation parameters.

2. Modeling

All symbols are listed in “Nomenclature”.

2.1. Proposed VOF-based method

We consider two immiscible and incompressible phases involving the electrolyte as the surrounding fluid, and the deposit as the solid phase. Hirt and Nichols [23] originally proposed the VOF method to simulate gas–liquid and liquid–liquid multiphase systems. Thus, using VOF for simulating the solid deposit requires additional assumptions and considerations that will be further elucidated in “2.3. Transport phenomena within the deposit”. The two phases are identified using a spatial and temporal-dependent marker function (β),

$$\beta(\vec{x}, t) = \frac{V_{\mathrm{d}}}{V} = \begin{cases} 1, \vec{x} \in \mathit{Deposit} \\ 0 < \beta < 1, \ \vec{x} \in \mathit{Interface} \\ 0, \vec{x} \in \mathit{Electrolyte} \end{cases} \tag{1}$$

An advection equation for β is solved on a fixed Eulerian grid,

$$\frac{\partial \beta}{\partial t} + \nabla\cdot(\beta u) = \frac{\dot{m}}{\rho_{\mathrm{d}}}. \tag{2}$$

The mass source term ($\dot{m}$) determines the local growth of the cathode surface,

$$\dot{m} = \frac{a_{\mathrm{VOF}} M}{zFV}(\vec{j}\ .\ \vec{n}) \tag{3}$$

Calculations of $\vec{n}$ and a_{VOF} are discussed in “2.2. Computation of the interface area”.

The mass transfer is only at the interface cells ($0 < \beta < 1$), and the interface shifts to the next neighboring computational cell after completion of deposition ($\beta = 1$).

Continuity and momentum equations determine the flow field,

$$\nabla\cdot u = \dot{m}\left(\frac{1}{\rho_{\mathrm{d}}} - \frac{1}{\rho_{\mathrm{e}}}\right) \tag{4}$$

$$\frac{\partial \rho u}{\partial t} + \nabla\cdot(\rho u u) = -\nabla p + \nabla\cdot[\mu(\nabla u + \nabla u^{\mathrm{T}})] + \rho g \tag{5}$$

where $\rho = \beta\rho_{\mathrm{d}} + (1-\beta)\rho_{\mathrm{e}}$ and $\mu = \beta\mu_{\mathrm{d}} + (1-\beta)\mu_{\mathrm{e}}$ are weighted-average of phases occupying each computational cell.

Laplace equation determines the electrolyte potential (φ) field,

$$\nabla\cdot(-\kappa\nabla\varphi) = 0 \tag{6}$$

where $\vec{j} = -\kappa\nabla\varphi$.

2.2. Computation of the interface area

$\vec{n}$ and a_{VOF} are computed at each time step to accurately evaluate $\dot{m}$ in Eq. (3) aiming at ensuring mass conservation using the following proposed algorithm designed only for quadrilateral square shaped mesh elements in the deposit region. $\vec{n} = (n_{\mathrm{x}}, n_{\mathrm{y}})$ is given by: $\vec{n} = \frac{\vec{\nabla}\beta}{\|\vec{\nabla}\beta\|}$ and a_{VOF} is bounded ($a_{\mathrm{VOF}} = [0, \sqrt{2}a]$). As shown in Fig. 2, three situations are plausible. In situation (I), the absolute value of one of the components of the unit normal vector is equal to one ($|n_{\mathrm{x}}| = 1$ or $|n_{\mathrm{y}}| = 1$) where $a_{\mathrm{VOF}} = a$. In situation (II), the interface connects two perpendicular sides of the cell so that β is the area of a triangle in 2D. Contrastingly, the interface connects two parallel sides of the cell in situation (III), whereby β is the area of a trapezoid in 2D. To distinguish between situation (II) and situation (III), the limit volume fraction (β_{L}) is calculated:

$$\beta_{\mathrm{L}} = \frac{\tan\theta}{2} = \min\left(\frac{|n_{\mathrm{y}}|}{2\ |n_{\mathrm{x}}|}, \frac{|n_{\mathrm{x}}|}{2\ |n_{\mathrm{y}}|}\right) \tag{7}$$

Eventually, a_{VOF} for situations (II) and (III) is:

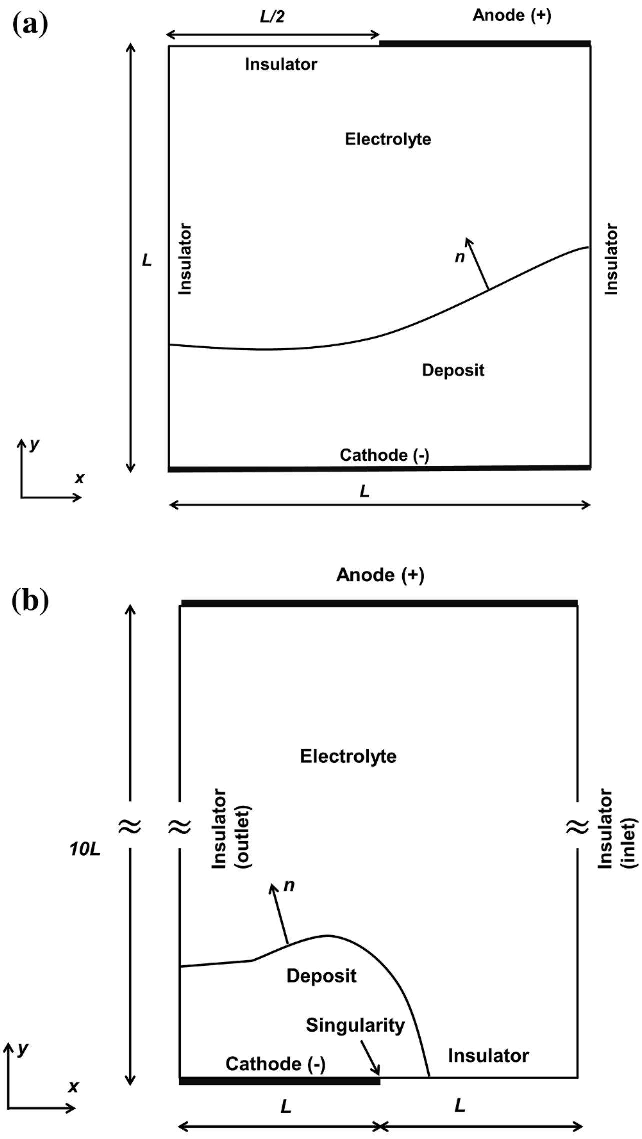

Fig. 1. Two cases are studied. Geometrical parameters related to computational domains are given. Vector $\vec{n}$ indicates the normal direction to the deposit front: (a) unidirectional electrodeposition; (b) multidirectional electrodeposition.

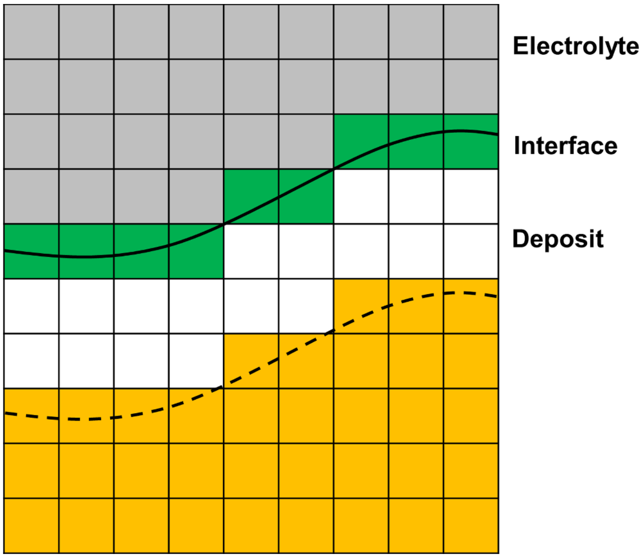

Fig. 3. The computational domain is divided into four group of cells that is schematically shown: electrolyte (grey cells), interface (green cells), and deposit (white and yellow cells). Note that the mesh resolution is shown exaggeratedly coarse for illustrative purposes. (For interpretation of the references to colour in this figure legend, the reader is referred to the web version of this article.)

Table 1
Parameters used in our calculations.

Parameter	
R [J $\text{K}^{-1}\text{mol}^{-1}$]	8.314546
T [K]	293
ρ [kg m^{-3}]	1000
μ [Pa s]	0.001
M [g mol^{-1}]	63.55
F [A s mol^{-1}]	96,485
κ [S m^{-1}]	5.1
j_0 [A m^{-2}]	5
L [cm]	1
u_0 [cm s^{-1}]	0.001
z	2
α	0.5
I_0	1
$\bar{\varphi}$	1 and 3.87

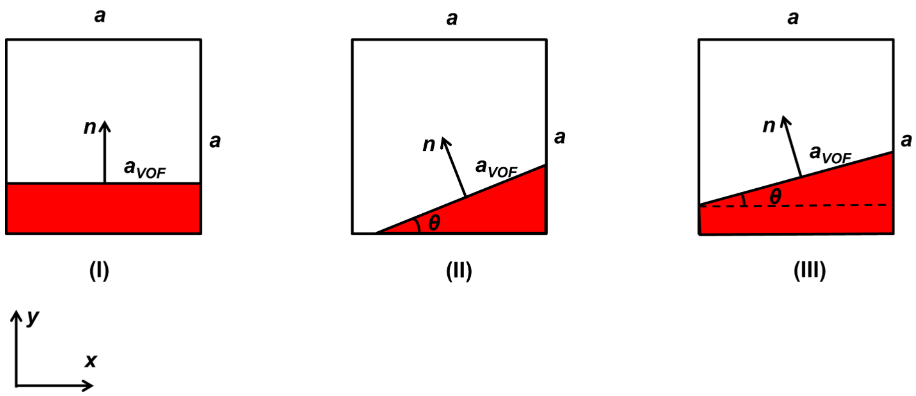

Fig. 2. All possible situations (I, II, and III) which are considered to compute the VOF interface area are illustrated. The red zone demonstrates the area filled by deposit. (For interpretation of the references to colour in this figure legend, the reader is referred to the web version of this article.)

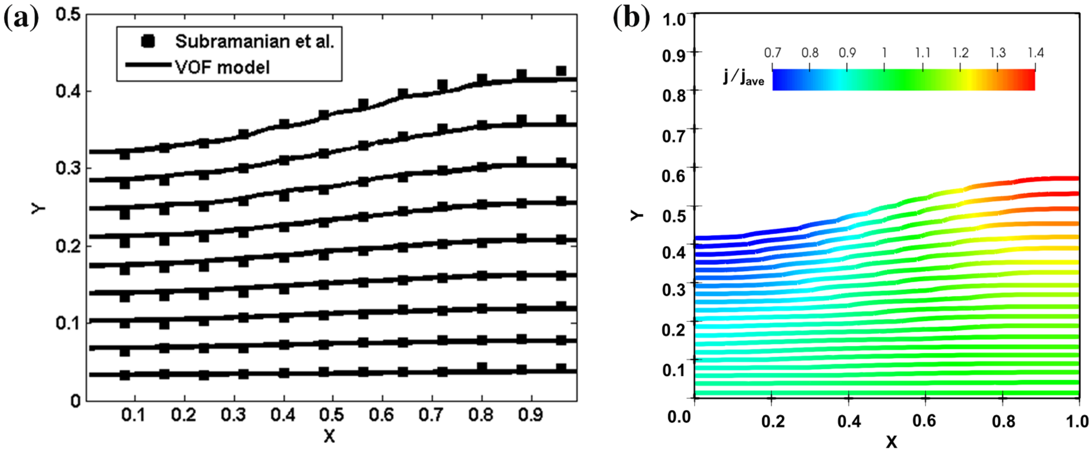

Fig. 4. The abscissa and ordinate are dimensionless. (a) A comparison is made between our modeling results and results obtained by Subramanian and White [28] to capture the evolution of deposit front; (b) The contour-plot of normalized electric current density ($\frac{j}{j_{\mathrm{ave}}}$) on the deposit front.

$$a_{\mathrm{VOF}} = \begin{cases} \sqrt{\frac{2\beta a^2}{|n_{\mathrm{x}}|\,|n_{\mathrm{y}}|}}, & 0 < \beta < \beta_{\mathrm{L}} \\ \min\left(\frac{a}{|n_{\mathrm{x}}|}, \frac{a}{|n_{\mathrm{y}}|}\right), & \beta_{\mathrm{L}} < \beta < 1 - \beta_{\mathrm{L}} \\ \sqrt{\frac{2(1-\beta)a^2}{|n_{\mathrm{x}}|\,|n_{\mathrm{y}}|}}, & \beta_{\mathrm{L}} < \beta < 1 \end{cases} \tag{8}$$

A detailed derivation is provided in the supplemental materials as “VOF-Interface-Area.pdf”.

2.3. Transport phenomena within the deposit

The computational domain is divided into four groups of cells (Fig. 3) including the deposit (white and yellow cells), the interface (green cells) and the electrolyte (grey cells). The velocity must become zero within the deposit and at the interface, since the deposit front (interface) only moves forward as a consequence of converting ions in the electrolyte to atoms at the interface through Eq. (3). Increasing the viscosity by a factor of ca. 100 times helps to significantly reduce the velocity [30]. Additionally, a sink term is included in Eq. (5) to completely cease flow in white, yellow and green cells,

$$S_{\mathrm{u}} = -\frac{\mu}{K}\beta u \tag{9}$$

Simulation trials revealed that any value of K in the range of 10^{-6} to 10^{-10} is suitable. Of note, using a very small value (e.g. 10^{-20}) may lead to numerical instability and lack of convergence.

Previously, we pointed out that the shape of deposit front could be accurately captured with or without including calculations of field structures inside the deposit region considering secondary current distribution [21]. Generally, the electrical conductivity of the deposit (metal) is several orders of magnitudes larger than that of the electrolyte. Therefore, the electric field (gradient of potential) is minimal within the deposit. Similar to Eq. (9), a sink term is applied in Eq. (6) in yellow cells to suppress the potential,

$$S_{\varphi} = -\frac{\beta\varphi}{K} \tag{10}$$

The front of region involving yellow cells is located after a transitional layer (two or three white cells) behind the deposit front to avoid gradient jump over the interface.

Butler–Volmer (BV) kinetics considering secondary current distribution is given by,

$$j_{\mathrm{BV}} = j_0\,[e^{\frac{\alpha zF\varphi_{\mathrm{int}}}{RT}} - e^{-\frac{(1-\alpha)zF\varphi_{\mathrm{int}}}{RT}}] \tag{11}$$

Of note, Eq. (11) has been superseded in the latest IUPAC recommendations [31]. Herein, this equation form is retained for direct comparison to the legacy electrodeposition literature. BV condition is imposed at the interface (green cells) exploiting a variable spatial and temporal-dependent electrical conductivity considering discrete gradient estimation,

$$\kappa(\vec{x}, t) = \frac{j_{\mathrm{BV}}\,\delta}{\varphi_{\mathrm{int}}} \tag{12}$$

Eq. (12) is derived considering that j_{BV} is equivalent to the flux of charge at the interface. Considering the Green–Gauss cell-based gradient theorem [27], the length scale (δ) is the sum of cell sides ($4a$). Therefore, Eq. (6) in the entire domain together with Eq. (11) and Eq. (12) in the green zone are executed in an iterative procedure at each time step to update magnitudes of $\vec{j}$, φ and $\kappa(\vec{x}, t)$ aiming at achieving the converged transient solution.

2.4. Other settings

All modeling equations are implemented in the commercial CFD software, ANSYS FLUENT v.17.1, using user-defined functions (UDF). Models were configured based on studies conducted by Subramanian et al. [28], Alkire et al. [10], and Zamani et al. [12]. Accordingly, potential field is solved in dimensionless form to compare our VOF-based results with their results aiming at verification of our model. Dimensionless parameters are: $X = \frac{x}{L}$, $Y = \frac{y}{L}$, $\bar{\varphi} = \frac{zF\varphi}{RT}$, $I_0 = \frac{j_0 LnF}{\kappa RT}$. The dimensionless forms of the equations are described in details in Refs. [10,12,28].

The first computational domain, Fig. 1(a), corresponding to the study of Subramanian et al. [28] namely unidirectional contains 10,000 structured equisized elements with the size of 0.1 mm. The second computational domain, Fig. 1(b), corresponding to the study of Alkire et al. [10], and Zamani et al. [12] namely multidirectional contains 45,000 quadrilateral square shaped mesh elements with the size of 0.06 mm in a rectangular zone ($2L$ in the x-direction and $0.5L$ in the y-direction) near cathode where deposition takes place. The mesh size is gradually and incrementally increased away from the rectangular zone toward the anode considering a successive ratio of 5%.

The temporal and spatial discretization schemes are first-order implicit and third-order MUSCL [27,32]. The explicit scheme to discretize β in Eq. (2) is Geo-Reconstruct [33].

The flux of potential is set to zero at insulators. The value of potential is set zero at cathode. Electrodeposition can take place under potentiostatic (constant potential) or galvanostatic (constant electric current) condition [34]. Herein, the potential at anode is given considering potentiostatic mode: unidirectional ($\bar{\varphi} = 1$), and multidirectional ($\bar{\varphi} = 3.87$). Extension of the model to galvanostatic mode is

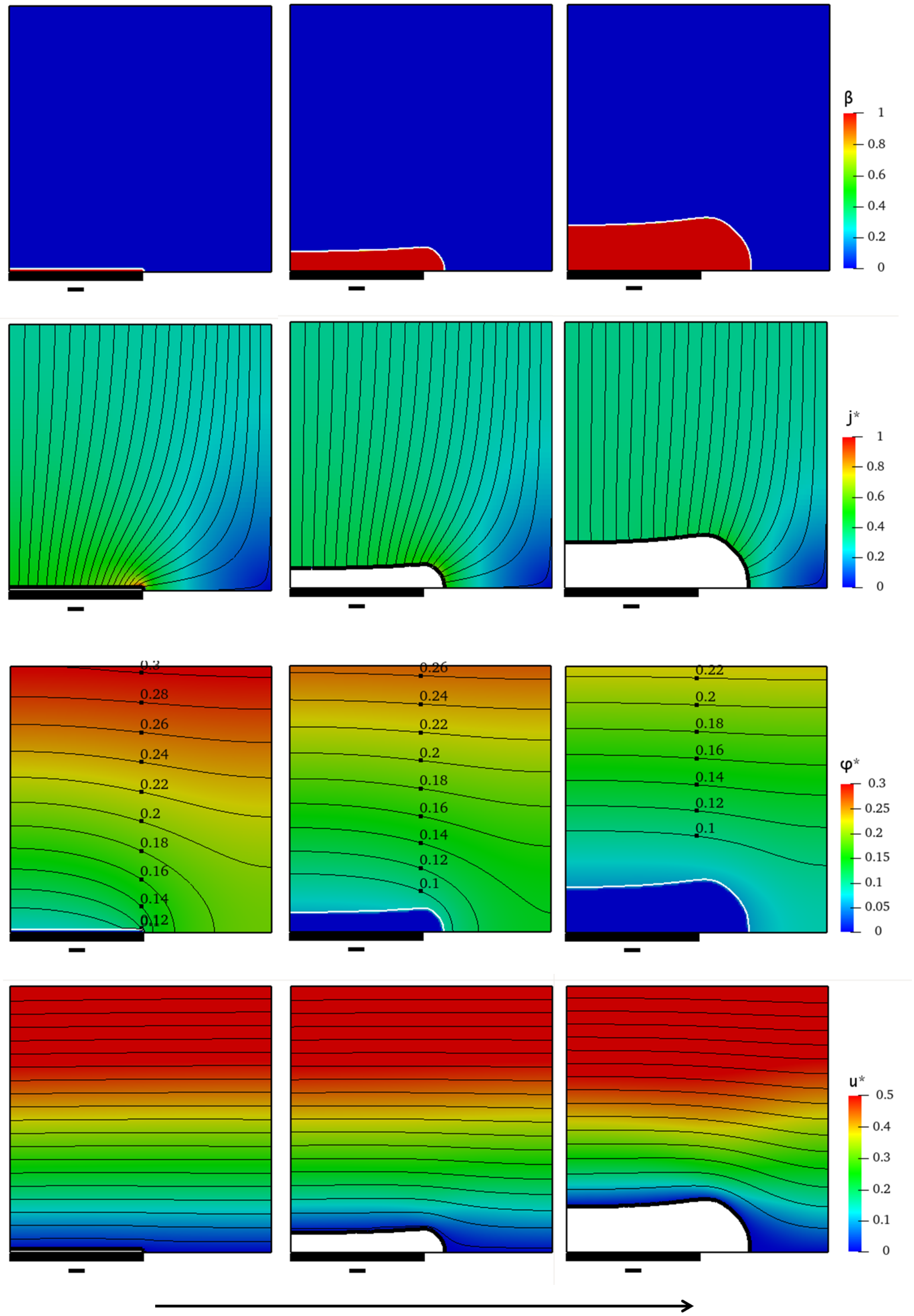

Fig. 5. Snapshots at different times of the field structures in the region near cathode are shown: (First row) volume fraction of deposit (β), (second row) the magnitude and streamlines of normalized electric current density (j^*), (Third row) contour of normalized potential and normalized equipotential surfaces (φ^*), (Fourth row) the magnitude and streamlines of normalized velocity (u^*). The arrow indicates time-advancement.

a topic for future work. The flow of electrolyte is only computed in the multidirectional shape change, Fig. 1(b), where pressure-outlet (imposition of a constant pressure) is assigned as boundary condition for flow at outlet. The pressure gradient is zero at all other boundaries. The velocity at inlet is assigned according to the laminar parabolic flow between two parallel planes: $u = \frac{6u_0 y}{(10L)^2}(10L - y)$. All parameters are listed in Table 1. Of note, CFL number, $\frac{\Delta t}{a}\max(u, u_{\mathrm{df}})$, where $u_{\mathrm{df}} = \left(\frac{M}{zF\rho}\vec{j}\ .\ \vec{n}\right)$ must be kept much smaller than one to ensure a converged solution. The computation time on a single processor Intel Core i7-4790 K CPU 4.00 GHz is ca. one hour.

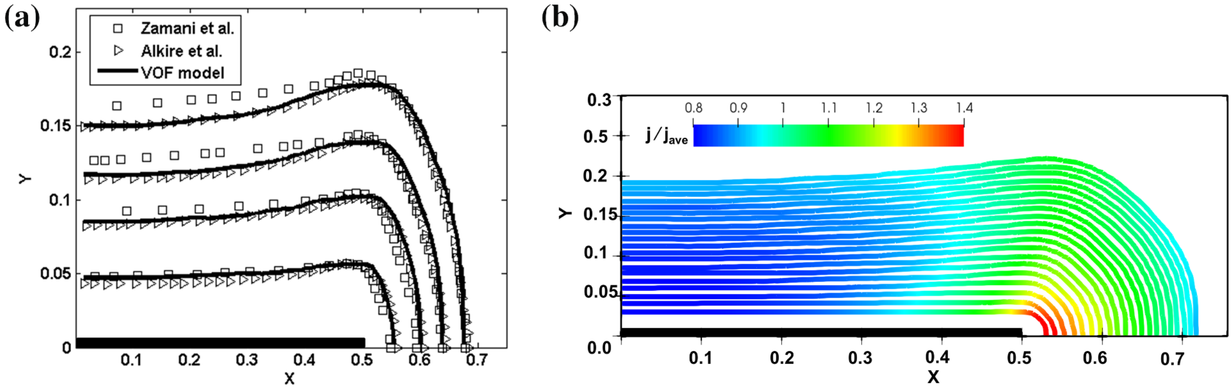

Fig. 6. The abscissa and ordinate are dimensionless. Original cathode shape is shown along abscissa using a black bar. (a) A comparison is made between our modeling results and results obtained by Alkire et al. [10] and Zamani et al. [12] to capture the evolution of deposit front; (b) The contour-plot of normalized electric current density ($\frac{j}{j_{\text{ave}}}$) on the deposit front.

3. Results and discussion

3.1. Unidirectional shape change

For the system shown in Fig. 1(a), semi-analytical solutions were previously presented by Subramanian and White [28]. The electrolyte velocity field is not computed; hence $\vec{u}$ is set zero in Eq. (2), and Eqs. (4), (5) are not solved. The electric current density flows from anode toward the cathode. As time proceeds, the deposit thickness increases and consequently the total electrical resistance of the system decreases. A higher amount of electrical current is permitted to flow through the system at constant applied voltage as the deposit front advances. As shown in Fig. 4(a), a good agreement is observed between our modeling results with analytical results considering the transient thickness of deposit layer. The variation in the magnitude of electric current density along the deposit front is an important factor to characterize the performance of the process. Conventionally, the ratio of electric current density to the average electric current density ($\frac{j}{j_{\text{ave}}}$) along the deposit front is utilized as shown in Fig. 4(b) using contour-plot. As the deposit front moves forward, the ratio increases which implies that the non-uniformity of the thickness of the deposit layer amplifies. All transient results are provided in supplemental materials as “Unidirectional.avi”.

3.2. Multidirectional shape change

Here, the system represents the well-known electroforming process for copper with overgrowing of the insulator in the vicinity of the electrode [29]. The highly non-uniform electric current density distribution adjacent the sharp corner of electrode-insulating substrate is transferred to a remarkable non-uniform deposition layer. Demonstratively, snapshots at different times of the field structures are shown in Fig. 5. As anticipated, the maximum amount of electric current density is near the singularity. As time proceeds, the area of deposit front increases and consequently the electric current density at the deposit front decreases. The trajectory of electric current density is illustrated using streamlines of electric current. The flux of potential is specified through BV equation at the very deposit-electrolyte interface where the electric current density is perpendicular to the deposit front. However, a noteworthy amount of the electric current density flows tangential to deposit front so that the streamlines do not appear perpendicular to the interface. The equipotential surfaces are perpendicular to the streamlines of electric current density at each point inside the electrolyte. They perpetually re-locate as the deposit front moves forward. The inlet velocity is given to ensure the flow is laminar which is associated with Reynolds number equal to one ($Re = 1$). The impact of concentration fields of ions which is driven by flow on the electric field is ignored in the calculation of secondary current distribution. Therefore, variations in the flow field has no influence on the shape of deposit front. However, the growth of deposit layer shifts the position of the hydrodynamic boundary layer near the wall as shown in Fig. 5. Results are illustrated in supplemental materials as “Multidirectional.avi”, and “Cathode-growth.avi”. Evaluation of the overall mass and charge conservation is provided as “Conserve-mass.pdf”.

The computed profile of the deposit front is compared to results obtained by previous studies [10,12] as shown in Fig. 6(a). A very good agreement is observed. Fig. 6(b) illustrates the contour-plot of ($\frac{j}{j_{\text{ave}}}$) along the deposit front. As deposit front moves forward, the ratio decreases that is in favor of producing a uniform deposition layer. In other words, the amplitude of non-uniformity in the distribution of electric current density along the deposit front diminishes as the thickness of deposition layer grows. This implies that it is essential to minimize the overshoot in the amount of electric current density at the singularity in the initial stages of the growing deposit to obtain a uniform deposit layer.

4. Summary

We propose a novel approach using the volume of fluid method (VOF) to simulate transient shape change of the deposit front during electrodeposition. The model is examined on two-dimensional systems for which mathematical solutions are available. Field structures such as electrolyte potential, electric current density, and flow of electrolyte are computed considering secondary current distribution. The VOF interface in each computational cell moves at each time step as a consequence of mass transfer during electrodeposition. A novel algorithm is suggested to compute the exact area of VOF interface. Proper modeling equations are suggested to accurately handle transport phenomena within the deposit. The method is then utilized to model electroforming of copper in the presence of edge effects at the singularity between the cathode and insulator. As the deposit front moves forward, the impact of the edge effects on the thickness of the deposit layer becomes weaker. As such, the overshoot of electric current density at the singularity in initial stages must be minimized to obtain a uniform deposition layer and consequently to improve the performance of the process. All transient results are shown through animations in supplemental materials.

CRediT authorship contribution statement

E. Karimi-Sibaki: Conceptualization, Methodology, Software, Writing - original draft. **A. Kharicha:** Conceptualization, Methodology, Supervision, Writing - review & editing. **A. Vakhrushev:** Visualization, Writing - review & editing. **M. Wu:** Supervision. **A. Ludwig:** Supervision. **J. Bohacek:** Methodology, Software.

Declaration of Competing Interest

The authors declare that they have no known competing financial interests or personal relationships that could have appeared to influence the work reported in this paper.

Acknowledgements

The authors acknowledge financial support from the Austrian Federal Ministry of Economy, Family and Youth and the National Foundation for Research, Technology and Development within the framework of the Christian-Doppler Laboratory for Metallurgical Applications of Magnetohydrodynamics.

Appendix A. Supplementary data

Supplementary data (https://smmp.unileoben.ac.at/de/2711/) to this article can be found online at https://doi.org/10.1016/j.elecom.2020.106675.

References

[1] Y.D. Gamburg, G. Zangari, Theory and Practice of Metal Electrodeposition, Springer-Verlag, New York, 2011.
[2] M. Paunovic, M. Schlesinger, Fundamentals of Electrochemical Deposition, Wiley, New York, 1998.
[3] M. Rosales, J.L. Nava, J. Electrochem. Soc. 164 (2017) E3345–E3353.
[4] C.M. Patil, K.S.V. Santhanam, S.G. Kandlikar, Int. J. Heat Mass Transf. 79 (2014) 989–1001.
[5] G. Mutschke, A. Bund, Electrochem. Commun. 10 (2008) 597–601.
[6] J.O. Dukovic, IBM J. Res. Develop. 34 (1990) 693–705.
[7] E.J.F. Dickinson, H. Ekström, E. Fontes, Electrochem. Commun. 40 (2014) 71–74.
[8] E. Karimi-Sibaki, A. Kharicha, M. Wu, A. Ludwig, J. Bohacek, J. Electrochem. Soc. 165 (2018) E604–E615.
[9] J. Newman, K.E. Thomas-Alyea, Electrochemical Systems, John Wiley & Sons, New Jersey, 2004.
[10] R. Alkire, T. Bergh, R.L. Sani, J. Electrochem. Soc. 125 (1978) 1981–1988.
[11] A. Mahapatro, S. Kumar Suggu, Adv. Mater. Sci 3 (2018) 1–9.
[12] N.G. Zamani, F.H. Peters, Appl. Math. Model. 10 (1986) 262–265.
[13] D. Wheeler, D. Josell, T.P. Moffat, J. Electrochem. Soc. 150 (2003) C302–C310.
[14] M. Hughes, N. Strussevitch, C. Bailey, K. McManus, J. Kaufmann, D. Flynn, M.P.Y. Desmulliez, Int. J. Numer. Meth. Fluids 64 (2010) 237–268.
[15] D. Adalsteinsson, J.A. Sethian, J. Comput. Phys. 122 (1995) 348–366.
[16] M. Georgiadou, D. Veyret, R.L. Sani, R.C. Alkire, J. Electrochem. Soc. 148 (2001) C54–C58.
[17] W. Pongsaksawada, A.C. Powell IV, D. Dussault, J. Electrochem. Soc. 154 (2007) F122–F133.
[18] D.A. Cogswell, Phys. Rev. E 92 (2015) 011301(R).
[19] T.O. Drews, S. Krishnan, J.C. Alameda, D. Gannon, R.D. Braatz, R.C. Alkire, IBM J. Res. Develop. 49 (2005) 49–63.
[20] C. Lupo, D. Schlettwein, J. Electrochem. Soc. 166 (2019) D3182–D3189.
[21] E. Karimi-Sibaki, A. Kharicha, M. Abdi, M. Wu, A. Ludwig, J. Bohacek, J. Electrochem. Soc. 166 (2019) D521–D529.
[22] M. Schanz, Wave Propagation in Viscoelastic and Poroelastic Continua, Springer, 2001.
[23] C.W. Hirt, B.D. Nichols, J. Comput. Phys. 39 (1981) 201–225.
[24] O. Ubbink, Numerical Prediction of Two Fluid Systems with Sharp Interfaces, Ph.D. Thesis Imperial College of Science, Technology and Medicine, 1997.
[25] A. Kharicha, M. Wu, A. Ludwig, E. Karimi-Sibaki, Metall. Mater. Trans. B 47 (2016) 1427–1434.
[26] M.R. Davidson, M. Rudman, J. Numeric, Heat Transf., Part B: Fundam. 41 (2002) 291–308.
[27] F. Moukalled, L. Mangani, M. Darwish, The Finite Volume Method in Computational Fluid Dynamics, Springer International Publishing, Switzerland, 2016.
[28] V.R. Subramanian, R.E. White, J. Electrochem. Soc. 149 (2002) C498–C505.
[29] M. Purcar, J. Deconinck, B. Van den Bossche, L. Bortels, Eur. Phys. J. Appl. Phys. 39 (2007) 85–94.
[30] S. Sasic, E. Karimi Sibaki, H. Ström, Eur. J. Mech. B Fluids 43 (2014) 65–75.
[31] R. Guidelli, R.G. Compton, J.M. Feliu, E. Gileadi, J. Lipkowski, W. Schmickler, S. Trasatti, Pure Appl. Chem. 86 (2014) 259–262.
[32] B. van Leer, J. Comput. Phys. 32 (1979) 101–136.
[33] D.J. Benson, Appl. Mech. Rev. 55 (2002) 151–165.
[34] P. Los, A. Lukomska, S. Kowalska, M. Kwartnik, J. Electrochem. Soc. 161 (2014) D593–D599.